

## Geology

### Microseismic measurement of wave-energy delivery to a rocky coast

Peter N. Adams, Robert S. Anderson and Justin Revenaugh

*Geology* 2002;30;895-898

doi: 10.1130/0091-7613(2002)030<0895:MMOWED>2.0.CO;2

---

**Email alerting services** click [www.gsapubs.org/cgi/alerts](http://www.gsapubs.org/cgi/alerts) to receive free e-mail alerts when new articles cite this article

**Subscribe** click [www.gsapubs.org/subscriptions/](http://www.gsapubs.org/subscriptions/) to subscribe to *Geology*

**Permission request** click <http://www.geosociety.org/pubs/copyrt.htm#gsa> to contact GSA

Copyright not claimed on content prepared wholly by U.S. government employees within scope of their employment. Individual scientists are hereby granted permission, without fees or further requests to GSA, to use a single figure, a single table, and/or a brief paragraph of text in subsequent works and to make unlimited copies of items in GSA's journals for noncommercial use in classrooms to further education and science. This file may not be posted to any Web site, but authors may post the abstracts only of their articles on their own or their organization's Web site providing the posting includes a reference to the article's full citation. GSA provides this and other forums for the presentation of diverse opinions and positions by scientists worldwide, regardless of their race, citizenship, gender, religion, or political viewpoint. Opinions presented in this publication do not reflect official positions of the Society.

---

#### Notes

# Microseismic measurement of wave-energy delivery to a rocky coast

Peter N. Adams } Department of Earth Sciences, University of California, Santa Cruz, California 95064, USA

Robert S. Anderson } Department of Earth Sciences and Center for the Study of Imaging and Dynamics of the Earth,

Justin Revenaugh } University of California, Santa Cruz, California 95064, USA

## ABSTRACT

Rocky coasts are attacked by waves that drive sea-cliff retreat and etch promontories and embayments into the coastline. Understanding the evolution of such coastlines requires knowledge of the energy supplied by waves, which should depend upon both the deep-water waves and the coastal bathymetry they cross. We employ microseismic measurements of the wave-induced shaking of sea cliffs near Santa Cruz, California, as a proxy for the temporal pattern of wave-energy delivery to the coast during much of the winter 2001 storm season. Visual inspection of the time series suggests that both deep-water wave heights and tide levels exert considerable control on the energy delivered. We test this concept quantitatively with two models in which synthetic time series of wave power at the coast are compared with the shaking data. In the first model, deep-water wave power is linearly scaled by a fitting parameter; because this model fails to account for the strong tidal signal, it fits poorly. In the second model, the wave transformation associated with shoaling and refraction diminishes the nearshore wave power, and dissipation associated with bottom drag and wave breaking is parameterized by exponential dependencies on two length scales; this model reduces the variance by 32%–45% and captures the essence of the full signal. Shoaling and refraction greatly modulate the wave power delivered to the coast. Energy dissipated by bottom drag across the shelf is relatively small; the dissipation length scale is many times the path length across the shelf. In contrast, much energy is dissipated in the surf zone; the tidal-dissipation depth scale is of the same order as the tidal range (1–2 m), which accounts for the strong dependence of the cliff shaking on the tide.

**Keywords:** microseismic methods, coastal geomorphology, waves, energy.

## INTRODUCTION

The morphology of a rocky coast along a tectonically active margin results from the interaction of uplifted resistant coastal bedrock and the destructive energy delivered to the coast by waves. Rocky coasts inspire interesting geomorphic questions about embayment shape, marine terraces, and the relative roles of climate and lithology in coastline evolution. Lithology of coastal sea cliffs provides one control on rocky coast evolution and offshore ocean climate provides another. Storm systems generate waves whose power is reduced by energy dissipation during shoaling; the remaining power is expended in the surf zone and at the sea cliffs (Komar, 1998). As a first step toward addressing rocky coast evolution, we explore the utility of seismically sensed shaking of the sea cliffs as a measure of how offshore wave conditions, shelf bathymetry, and tides dictate the delivery of geomorphically useful energy to a rocky coast.

Deep-water waves begin losing energy through friction when their orbital motions extend to the seafloor (Fig. 1). Long-period waves and those occurring at low tide sense the seafloor farther offshore and dissipate a greater fraction of deep-water energy than do short-period waves or those occurring at high tide. The deep-water swell direction and refraction of a wave's ray path dictate the length of wave travel during which energy is dissipated. Wave power is also diminished by stretching of wave crests during refraction. In essence, deep-water wave power,  $P_0$ , is transformed into delivery power,  $P_D$ , through a filter that depends on bathymetry and several oceanographic variables. Here we attempt to characterize this filter by using a novel method.

Seismologists have long recognized that microseisms complicate measurements of earthquakes (Longuet-Higgins, 1950; O'Hanlon, 2001). Standing waves on the shelf generate a seismic signal from the constructive interaction of waves reflected from the coast with incoming waves of the same period. Ground motions from the breaking of

nearshore surf have also been noted. Microseisms may be distracting to the seismologists, but they are useful to oceanographers as a proxy for wave height, and they provide a record of ground motion in response to wave breaking. Zopf et al. (1976) demonstrated that microseisms could be used to measure wave heights when conventional pressure sensors are unavailable. Tillotson and Komar (1997) compared microseismically measured wave heights to those measured by buoys. Researchers have employed historical seismographic records to hind-cast (i.e., statistically predict past) changes in wave climate in the northeast Pacific (Bromirski et al., 1999) and in the North Atlantic (Grevemeyer et al., 2000). To date, however, few studies of coastal geomorphology have employed this valuable data source.

We assembled time series of wave heights and periods to characterize deep-water wave power, and swell directions and tidal elevations to calculate expected energy dissipation. These data were ob-

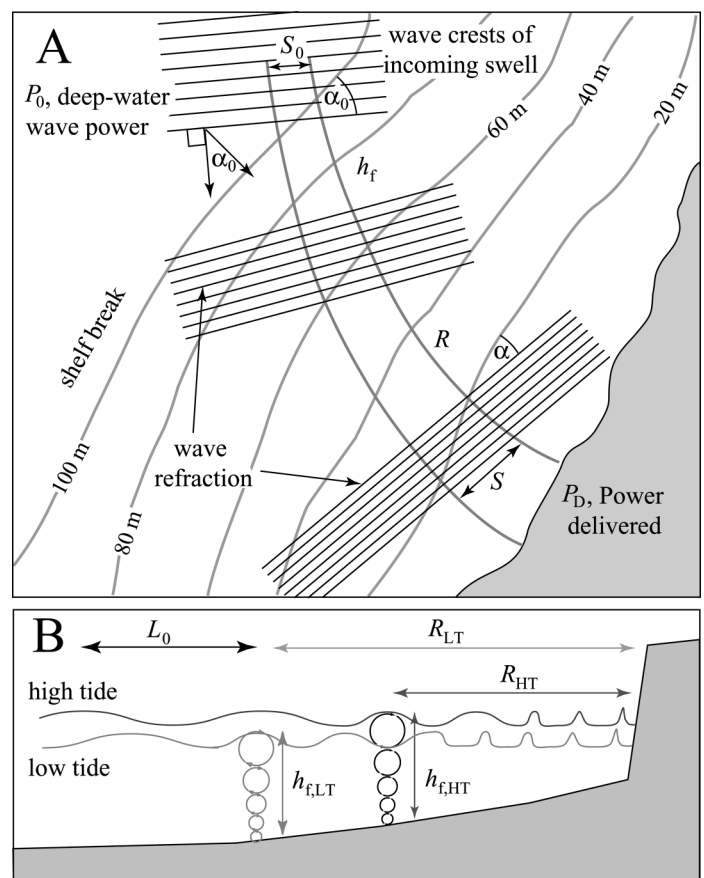


**Figure 1.** Definition sketch of variables controlling delivery power. **A:** Map view of wave transformation as wave group follows a refracting path toward shore. Note that wavelength shortens and refraction spreads crest length  $S_0$  to  $S$  as waves approach shore. Dissipation by bottom drag occurs once wave reaches depth  $h_f = L_0/2$  along length  $R$  before reaching highly dissipative surf zone.  $\alpha_0$  and  $\alpha$  are angles between wave crests and depth contours in deep water and breaking-wave depth in shallow water, respectively. **B:** Shore-normal cross section showing waves of wavelength  $L_0$  transforming toward shore at two tidal positions, HT (high tide, dark gray lines) and LT (low tide, light gray lines). Tidal elevation controls where wave orbitals begin to interact with seafloor at depths of  $h_{f,HT}$  and  $h_{f,LT}$  and at dissipative lengths,  $R_{HT}$  and  $R_{LT}$ , for high and low tide, respectively.

tained from a National Data Buoy Center (NDBC) buoy that records deep-water wave statistics and from a National Oceanographic and Atmospheric Administration tidal gauge. We compared time series of oceanographic variables with cliff-shaking observations made with a portable broadband seismometer deployed at the edge of the sea cliff and coupled to the bedrock. We then attempted to define the combination of offshore wave climate and near-coast characteristics that best explains the shaking of the sea cliff.

### IDENTIFICATION OF OCEANOGRAPHIC VARIABLES

The delivery power,  $P_D$ , of waves is controlled by oceanographic variables and bathymetry. We had to characterize both the deep-water wave power,  $P_0$ , and how it is modified through transformation of the waves.

#### Deep-Water Wave Height

Deep-water wave height,  $H_0$ , should exert the greatest control on delivery power. The energy density,  $E_0$ , of a deep-water wave is given by

$$E_0 = \frac{1}{8} \rho g H_0^2 \quad (1)$$

where  $\rho$  is the density of seawater and  $g$  is gravitational acceleration.  $P_0$  is defined as the energy flux per unit length of wave crest averaged over one wave period (Sunamura, 1992; Komar, 1998),

$$P_0 = E_0 C_0 n = \frac{1}{8} \rho g C_0 n H_0^2 \quad (2)$$

where  $C_0$  is deep-water wave celerity and  $n$  describes the shape evolution of a wave as it shoals, a hyperbolic function whose value is 1/2 in deep water and 1 in shallow water. The transformation of waves as they interact with the shelf results in evolution of their height and celerity. These transformations involve changes in wave geometry in plan view and in cross section (Fig. 1).

#### Wave Shoaling

Airy wave theory assumes that in the absence of refraction and bottom friction, wave power is conserved from deep to shallow water. Changes in wave height must therefore result in changes of the opposite sign in celerity (equation 2). This wave-shape evolution can be expressed as a shoaling coefficient ( $K_S$ ), where  $H$  and  $C$  are the local wave height and celerity, computed at the breaking wave depth:

$$K_S = \frac{H}{H_0} = \sqrt{\frac{1}{2n} \frac{C_0}{C}} \quad (3)$$

#### Wave Refraction

As waves approach a coast obliquely, refraction bends the wave crests toward a more coast-parallel orientation. Wave crests can be significantly stretched (Fig. 1A), allowing straight-crested offshore waves to distribute their power to a coastline whose shape is irregular and of greater length. Wave-crest stretching decreases wave height, thereby decreasing wave power. This effect is captured in a refraction coefficient,  $K_R$ , that further transforms offshore wave height:

$$K_R = \frac{H}{H_0} = \sqrt{\frac{S_0}{S}} = \sqrt{\frac{\cos \alpha_0}{\cos \alpha}} \quad (4)$$

where  $S_0$  and  $S$  are the wave-crest lengths between two wave rays in deep and shallow water, respectively, and  $\alpha_0$  and  $\alpha$  are angles between wave crests and depth contours in deep water and breaking-wave depth in shallow water, respectively (Fig. 1A). Incorporating both shoaling and refraction, wave height at the coast can be expressed as:

$$H = H_0 K_S K_R \quad (5)$$

The ratio of the delivery power of waves to their deep-water power simplifies to

$$\frac{P_D}{P_0} = K_R^2 \quad (6)$$

### Energy Dissipation

Energy dissipation by bottom interaction is dictated by both the depth at which waves begin to feel bottom and the path length over which dissipation occurs (Anderson et al., 1999). Two oceanographic variables dictate the location at which waves first begin interacting with the seafloor: the wavelength,  $L$  (set by wave period,  $T$ ) and the tide. The water depth,  $h_f$ , to which there is significant wave orbital motion is  $\sim L/2$ . Wave period influences  $P_D$  by affecting the wavelength and therefore the water depth at which energy dissipation begins. From Airy wave theory, the wavelength is related to wave period through the dispersion equation (Komar, 1998):

$$L = \frac{g}{2\pi} T^2 \tan h \left( \frac{2\pi h}{L} \right) \quad (7)$$

where  $h$  is the water depth. In deep water the hyperbolic tangent function approaches unity, and the water depth at which dissipation begins increases as the square of the wave period:  $h_f = (g/4\pi)T^2$ . Longer period waves feel bottom earlier and should lose a larger fraction of their energy to bottom friction.

Waves approaching perpendicular to the bathymetric contours should lose the smallest fraction of their deep-water wave power. In addition, a lower shelf slope increases the ray-path length over which dissipation occurs. Ignoring refraction of the wave, the dissipative path length,  $R$ , varies inversely with both the slope of the shelf,  $\theta$ , and the angle between wave crests and bottom contours,  $\alpha_0$  (Fig. 1), and goes as the square of the wave period:

$$R = \frac{h_f}{\sin(\theta)\cos(\alpha_0)} = \frac{gT^2}{4\pi \sin(\theta)\cos(\alpha_0)} \quad (8)$$

Increases in wave period and deep-water approach angle, and decreases in shelf slope, should lower the fraction of deep-water wave power reaching the coast.

Tide affects water depth and therefore the offshore distance at which waves begin to dissipate energy (Trenhaile, 2000). At high tide, a deep-water wave travels farther unhindered by dissipative interaction with the bottom than at low tide and should result in greater energy imparted to the sea cliff (Fig. 1B). At low tide, waves break farther offshore, expending most of their energy in the surf zone, severely reducing the energy imparted to the cliffs. We sought quantification of these effects.

### STUDY SITE

Our study site is located on the edge of the 10-m-high, nearly vertical sea cliff that forms a promontory beside a pocket beach at the Joseph M. Long Marine Lab, west of Santa Cruz, California, on the northern coast of Monterey Bay (Fig. 2A). A bedrock platform is situated directly below the site, but is submerged during high and low tides. Waves break anywhere from the base of the cliff to 50 m in front of it, depending on the tide and wave height. The coast is characterized by 5–30-m-high sea cliffs and is decorated with irregularly spaced pocket beaches. Bathymetry is controlled by a 15-km-wide continental shelf trending northwest ( $\sim 305^\circ$ ), with an average slope of 0.01. Northwesterly swell dominates, with brief periods of southerly swell occurring in winter (Fig. 2B).

### MICROSEISMIC MEASUREMENT METHOD

Nearshore wave energies are derived from measurements with a broadband seismometer of ground velocity associated with cliff shaking. We attached a RefTek L4C3D 1 Hz velocity transducer to the bedrock at the base of the marine-terrace deposits atop the sea cliff during January–May of 2001 (days 22–155). The sensor recorded instantaneous ground velocity in vertical, north-south, and east-west directions at a sampling frequency of 50 Hz. The velocity data were squared to obtain energy per unit mass, then summed for each hour to yield a cumulative hourly shaking value for each direction of ground motion. This approach reduces the data from 540 000 to 3 points per h, the same interval over which wave and tidal data are reported.

### OBSERVED WAVE-ENERGY DELIVERY

Hourly shaking data for a typical eight days are plotted alongside tide, deep-water wave height, swell direction, and wave period in Fig-

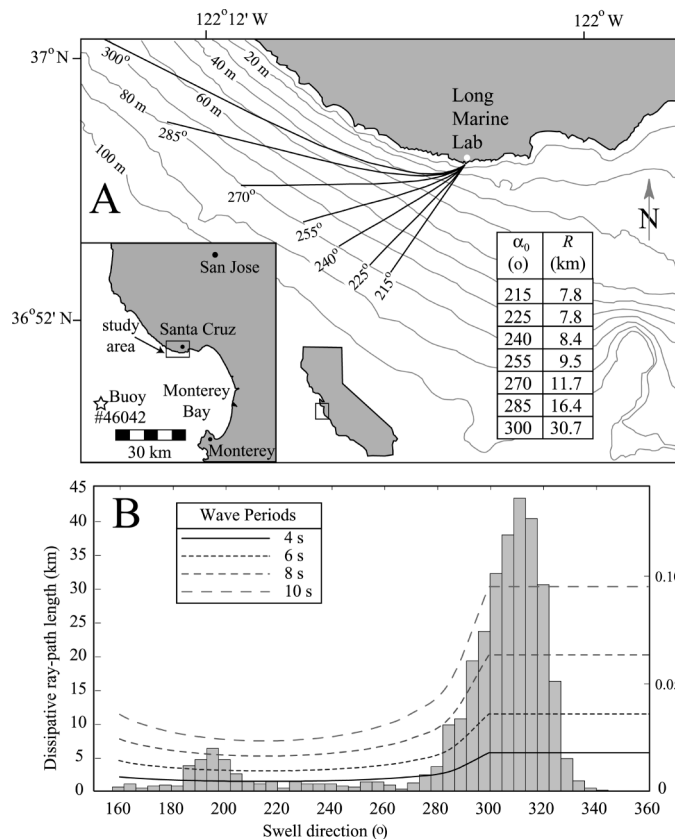


**Figure 2. A:** Setting for microseismic experiment, Long Marine Lab, Santa Cruz, California, north end of Monterey Bay. Refracted wave ray paths are shown for 10 s period wave ( $L_0 = 156$  m,  $h_t = 78$  m). Tabulated lengths show strong dependence upon swell direction. **B:** Histogram of deep-water swell directions (gray vertical bars; offshore buoy 46042) and dissipative ray-path lengths (solid and dashed lines) computed from refracting from depth  $h_t$  for four periods. Path lengths of waves from swells at  $>305^\circ$  are assumed to be similar to those coming essentially parallel to coast.

ure 3. Deep-water wave heights range from 0.7 m to 7.2 m, dominant wave periods from 3 s to 20 s, and swell directions from  $157^\circ$  to  $345^\circ$ ; the spring tidal range is  $\sim 2.5$  m. Maximum cliff-shaking energies for the entire time series are  $146 \mu\text{J}/\text{kg}$  (vertical),  $663 \mu\text{J}/\text{kg}$  (north-south), and  $1000 \mu\text{J}/\text{kg}$  (east-west). Peaks and troughs in tide are well correlated with those in shaking; cliff shaking intensifies during high tide. The shaking amplitude is strongly modulated by deep-water significant wave height.

### MODELING DELIVERY POWER OF WAVES

#### Simple Model

The simplest model of delivery power is a scaled version of deep-water wave power (equation 2):

$$P_{D1} = \beta P_0 \quad (9)$$

where  $\beta$  is a scaling factor representing the wave transformation, seismic attenuation, and geometric spreading of energy from the wave impact. It therefore includes the local effects of cliff height and lithology. Because it incorporates several factors,  $\beta$  has no significant meaning beyond a fitting parameter. This first model is compared to three separate eight-day periods of east-west ground motion in Figure 4. Although it captures the low-frequency behavior of the observed shaking, the amplitude of the signal at tidal periods is far underpredicted. Variance reductions from a baseline prediction of the mean of the shaking data are 11%, 3%, and 7% for the vertical, north-south, and east-west directions of ground motion, respectively. To account properly for the effects of shoaling, refraction, and frictional-energy dissipation, an advanced model must incorporate wave-height trans-

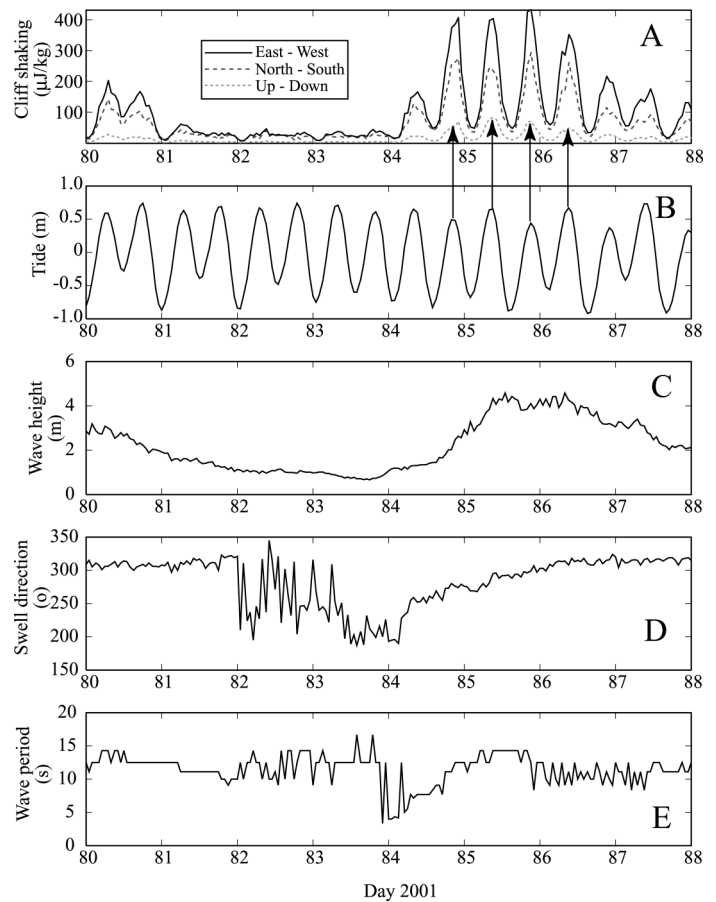


**Figure 3. Eight-day record from March 2001. A:** Microseismic shaking at cliff edge (three components of ground motion). **B:** Tidal elevation. **C:** Offshore significant wave height. **D:** Swell direction. **E:** Wave period. Horizontal shaking is considerably stronger than vertical. Note strong correspondence between times of high shaking and times of high tide (shown with arrows) over interval of large wave heights.

formation, tidal dependence, and the path length across the shelf traversed by the waves.

#### Effect of Shoaling and Refraction

Wave shoaling and refraction modify the delivery power by the fraction given in equation 6. Effective deep-water swell directions are computed assuming a Gaussian distribution with a mean set by the buoy data and a standard deviation of  $35^\circ$ . This allows us to treat waves whose mean swell direction is  $>90^\circ$  from coast normal. The computed wave ray path for each hour of data then yields a shoaling and refraction coefficient,  $\epsilon_{sr}$ , to modify wave power:

$$\epsilon_{sr} = \frac{P_D}{P_0} = K_R^2 \quad (10)$$

This coefficient ranges from 0.26 to 1.0 over the time series, indicating a strong dependence on wave shoaling and refraction.

#### Effect of Tides

The distance offshore,  $x$ , where maximum wave-energy dissipation occurs from wave breaking can be approximated as

$$x = D_0 - (b/\tan \theta) \quad (11)$$

where  $D_0$  is the distance from the sea cliff to the shoreline at lowest tide,  $b$  is the tide level above lowest tide, and  $\theta$  is the slope of the shelf. We explore an exponential dependence of the nearshore dissipation on tide.

$$\epsilon_t = e^{-x/D^*} \quad (12)$$

where  $D^*$  is a characteristic distance over which wave energy dissi-

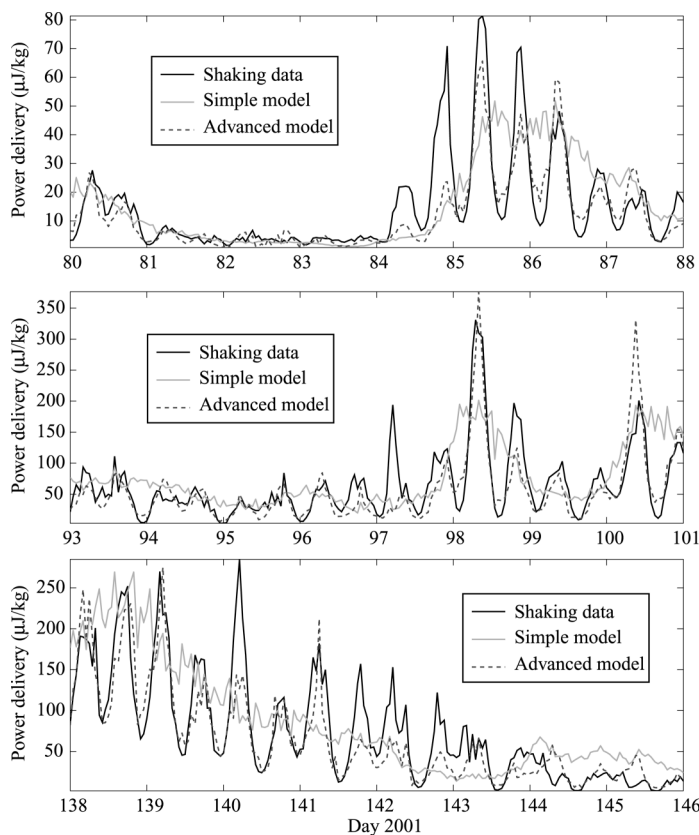


**Figure 4. Modeled time series of power delivery for three periods of eight days each, along with microseismic shaking (dark solid line). Note different scales of shaking magnitude for three plots. Simple model (light gray solid line) employs equation 9, whereas advanced model (dark gray dashed line)—incorporating wave shoaling and refraction, tide, dissipation from shelf drag, and temporally dependent seismic attenuation—uses equation 15.**

pates by a factor of  $e$ . Substituting equation 11 into equation 12 and converting the characteristic dissipation length into a characteristic water depth through  $b^* = D^* \tan \theta$ , the nearshore dissipation that explicitly accounts for tides may be written

$$\varepsilon_t = e^{-D_0/D^*} e^{b/b^*} \quad (13)$$

The value of  $\varepsilon_t$  varies between 0.08 and 1.0 over the observation period, indicating a strong dependence of shaking on tide, as suggested by visual inspection of the time series.

#### Effect of Ray-Path Length

To investigate the influence of dissipative ray-path length,  $R$ , we calculate the distance that a refracted wave travels over a shelf that is shallower than the orbital-interaction depth ( $h_f = L/2$ ), given the wave period and swell direction observed at the offshore buoy (Fig. 2).  $R$  is incorporated into a delivery-power modifier,  $\varepsilon_{rp}$ , as another exponential function, noting that an increase in  $R$  will decrease wave power delivered to the cliff:

$$\varepsilon_{rp} = e^{-R/R^*} \quad (14)$$

where  $R^*$  is a characteristic ray-path length. The ratio  $R/R^*$  is small throughout the time series, causing the normalized values of  $\varepsilon_{rp}$  to vary only from 0.84, 0.78, and 0.47 to 1.0 for the three directions of ground motion. Energy dissipation through bottom drag only weakly modulates the energy delivered to the sea cliffs.

#### Seasonally Variant Seismic Attenuation

We expect sea-cliff shaking to depend on water content of the cliff rock. Higher water content dampens shaking intensity. Ground-water content at our site is dominated by winter precipitation. Accord-

ingly, we introduce a simple, unitless, time-dependent seismic site-response parameter of the form  $(\beta + \gamma t)$ , where  $t$  is the fraction of the year and  $\beta$  and  $\gamma$  reflect the mean attenuation and its drift through the year, respectively.

#### Advanced Model

The advanced model includes the effects of wave shoaling and refraction, ray-path length, tides, and temporally dependent seismic attenuation:

$$P_D = (\beta + \gamma t) \varepsilon_{sr} \varepsilon_t \varepsilon_{rp} P_0 \quad (15)$$

and is solved using a nonlinear least-squares scheme for the constants  $\beta$ ,  $\gamma$ ,  $b^*$ , and  $R^*$ . This advanced model (Fig. 4) considerably improves the fit. Variance reductions from the mean baseline are 32%, 43%, and 45% for vertical, north-south, and east-west directions of ground motion, respectively, over the entire time series.

Over the three directions of ground motion,  $b^*$  varies by only 11% ( $b_{ud}^* = 1.12$  m,  $b_{ns}^* = 1.05$  m,  $b_{sw}^* = 1.18$  m). This result offers quantitative verification of the observation (Komar, 1998) that waves lose most of their energy upon breaking in the surf zone. These shallow depths also explain why the tidal signal is so strong in the shaking record: the characteristic dissipation depth ( $\sim 1$  m) is of the same order as the tidal range ( $\sim 2$  m). This similarity translates into a dissipation length  $D^*$  of  $\sim 100$  m. However, the characteristic dissipation length scale associated with bottom drag,  $R^*$ , is 110, 75, and 25 km for the three directions of ground motion, respectively. That the wave ray lengths,  $R$  ( $\sim 1$ –20 km; values given in Fig. 2A), are much less than these values suggests low dissipation by bottom drag.

#### CONCLUSIONS

Microseismic monitoring of wave-energy delivery to sea cliffs provides a rich data set against which to test theories of wave-energy dissipation. Given that seismologists working in coastal regions must commonly filter out the effects of waves, this is truly a case of one scientist's noise being another's signal. With a single stationary instrument, we were party to a natural experiment in which the effects of a wide set of oceanographic variables could be properly explored. Quantitative prediction of cliff shaking requires knowledge of these oceanographic variables and a model that accounts for (1) wave transformation due to shoaling and refraction and (2) dissipation through drag on the seafloor and through nearshore wave-breaking processes. We note that the tide strongly modulates the delivery of energy by controlling the location of wave break relative to the cliff. This experiment places on firmer footing any future modeling of long-term coastal evolution, including the generation of marine terraces and the embayment of coastlines.

#### ACKNOWLEDGMENTS

This work benefited from thoughtful reviews by Paul Komar and Brad Murray and was supported by a Friends of Long Marine Lab grant (to Adams) and National Science Foundation grant EAR-9803837 (to Anderson). The Southern California Earthquake Center provided seismic equipment, and Aaron Martin provided technical assistance. We thank Glenn Spinelli for field assistance, Susan Bilek for technical help, and Curt Storlazzi for numerous useful discussions. This is Center for the Study of Imaging and Dynamics of the Earth contribution 441.

#### REFERENCES CITED

- Anderson, R.S., Densmore, A.L., and Ellis, M.A., 1999, The generation and degradation of marine terraces: Basin Research, v. 11, p. 7–19.
- Bromirski, P.D., Flick, R.E., and Graham, N., 1999, Ocean wave height determined from inland seismometer data: Implications for investigating wave climate changes in the northeast Pacific: Journal of Geophysical Research, v. 104, p. 20753–20766.
- Grevenmeyer, I., Herber, R., and Essen, H.H., 2000, Microseismological evidence for a changing wave climate in the northeast Atlantic Ocean: Nature, v. 408, p. 349–352.
- Komar, P.D., 1998, Beach processes and sedimentation (second edition): Upper Saddle River, New Jersey, Prentice-Hall, Inc., 544 p.
- Longuet-Higgins, M.S., 1950, A theory of the origin of microseisms: Royal Society of London Philosophical Transactions, ser. A, v. 243, p. 1–35.
- O'Hanlon, L., 2001, Seismic sleuths: Nature, v. 411, p. 734–736.
- Sunamura, T., 1992, Geomorphology of rocky coasts: Chichester, Wiley and Sons, 302 p.
- Tillotson, K., and Komar, P.D., 1997, The wave climate of the Pacific Northwest (Oregon and Washington): A comparison of data sources: Journal of Coastal Research, v. 13, p. 440–452.
- Trenhaile, A.S., 2000, Modeling the development of wave-cut shore platforms: Marine Geology, v. 166, p. 163–178.
- Zopf, D.O., Creech, H.C., and Quinn, W.H., 1976, The wavemeter: A land-based system for measuring nearshore ocean waves: Marine Technological Society Journal, v. 10, p. 19–25.

Manuscript received February 15, 2002

Revised manuscript received June 13, 2002

Manuscript accepted June 18, 2002

Printed in USA